DOI: 10.24352/UB.OVGU-2017-003 TECHNISCHE MECHANIK, 36, 3, (2016), 166 – 179
submitted: April 15, 2016

A Stochastic Finite Element Method with a Deviatoric-volumetric Split for the Stochastic Linear Isotropic Elasticity Tensor

A. Dridger, I. Caylak, R. Mahnken

This paper presents a numerical method for solution of a stochastic partial differential equation (SPDE) for a linear elastic body with stochastic coefficients (random variables and/or random fields). To this end the stochastic finite element method (SFEM) is employed, which uses WIENER'S *polynomial chaos expansion in order to decompose the coefficients into deterministic and stochastic parts. As a special case, we consider isotropic material behavior with two fluctuating parameters. Computational approaches involving* GALERKIN *projection are applied to reduce the SPDE into a system of deterministic PDEs. Furthermore, we consider normally distributed random variables, which are assumed to be stochastically independent, and which establish the number of stochastic dimensions. Subsequently, the resulting finite element equation is solved iteratively. Finally, in a representative example for a plate with a ring hole we study the influence of different variances for material parameters on the variances for the finite element results.*

1 Introduction

In general, engineering structures exhibit heterogeneous materials, where adhesives, polycrystalline and composites are typical examples. The heterogeneity leads to uncertainty in the material parameters and, consequently, to uncertainty in the mechanical response. Therefore, macroscopically heterogeneous materials should be modelled by a stochastic rather than a deterministic approach. In addition, nowadays, hybrid materials are very popular. Due to the different types of attachments, uncertainties may occur especially at the interfaces of the material components. Thus, the computation of response statistics at the interfaces is one potential goal, which we want to address in the near future. Mathematically, such systems can be described by stochastic partial differential equations (SPDEs) with stochastic fields, which can be solved by the stochastic finite element method (SFEM).

There are two different approaches for SFEM in the literature: Firstly, the perturbation approach (Liu et al. (1986a,b); Wang et al. (2015)) which is based on a Taylor series expansion of the system response and secondly, as a more prominent approach, the spectral SFEM where *Polynomial Chaos Expansion* (PCE) and/or *Karhunen-Loève* (KL) expansions are introduced to represent random fields with a series of random *Hermite* polynomials (Feng et al. (2016); Ghanem and Spanos (1991); Keese (2004); Luo (2006); Matthies and Keese (2005); Sudret and Der Kiureghian (2000)). In this work, the second approach is favoured in which the stochastic input parameters and, accordingly, the system response are expanded with the PC expansion. The *Monte Carlo* (MC) simulation method (Hurtado and Barbat (1998); Papadrakakis and Papadopoulos (1996)) can also be combined to both approaches. Though characterized by its simplicity, however, it is expensive for large systems with an increasing number of input parameters or growth of the variances. Nevertheless, it is often used to investigate the accuracy of more advanced approaches. A detailed state-of-the-art review for stochastic finite element method can be found in Stefanou (2009).

The aim of this work is to consider the uncertainty of a linear elastic body using the SFEM, where an adhesive material is applied as a prototype. The uncertainty is considered by random material parameters, which are modelled as stochastic variables. These variables are expanded with PC and a *Galerkin* approach is used to solve the associated unknown coefficients of the solution. The key idea of our contribution is the split of the linear elasticity tensor into a volumetric and a deviatoric part in order to allow the analysis of the volumetric- and the deviatoric fluctuation. Then, from experimental data the distribution of the random variables, i.e. *Young's modulus* $E(\omega)$ and the *shear modulus* $G(\omega)$, are known. Consequently, E and G are expanded with PC, and a *Galerkin* projection,

see e.g. Ghanem and Spanos (1993); Matthies and Keese (2005), is applied to reduce the SPDE into a system of deterministic PDEs.

In a further part of this work, normally distributed material parameters are considered as stochastically independent input quantities for the stochastic process. To this end, two different cases are distinguished: In Case I $E(\omega)$ and $\nu(\omega)$ are given as two input parameters based on experimental data. Case II considers $G(\omega)$ to be given, instead of $\nu(\omega)$. The objective is the calculation of the uncertain system response (displacement). Another similar formulation to analyze the response displacement variability involving multiple uncertain material properties can be found in Graham and Deodatis (2001). Since, in both cases, additional elastic constants are calculated in dependence of the independent parameters, the number of stochastic dimensions is equal to the number of the independent input parameters. Finally, the stochastic finite element matrix equation consists of three contributions, namely the deterministic part as well as the variations of a volumetric and a deviatoric part.

An outline of this work is as follows: Section 2 summarizes the governing equations and the variational formulation for a linear elastic body with fluctuating material parameters. Section 3 and 4 provide respectively the spatial and the stochastic discretization. Then, in the representative example in Section 5 we consider two approaches (Case I and Case II) for a two parameter model of isotropic linear elasticity. To this end, we simulate a plate with a ring hole in plane strain subjected to uniaxial tension with the SFEM. Results of the deterministic solution as well as the influence of the distribution for the input parameters on the volumetric and deviatoric part are presented.

2 Basic Equations

2.1 Random Fields and Expected Value

For the subsequent exposition on the uncertainty of an elastic body, the following definitions are essential: Consider the probability space $(\Omega, \Sigma, \mathbb{P})$, where Ω is the set of elementary events, Σ is the σ-algebra and $\mathbb{P}$ is the probability measure. A *random variable* Z is a measurable function

$$Z\colon \Omega \longrightarrow V \tag{1}$$

where V is an appropriate measurable space (see Lasota and Mackey (1994) for more information). As an example, the uncertainty in the elasticity tensor $\boldsymbol{C}$ may be modelled by its definition as a function over the medium domain $R \subset \mathbb{R}^3$ as a random variable or more precisely, as a stochastic field Vanmarcke (1983):

$$\boldsymbol{C}\colon R \times \Omega \longrightarrow V,\ (\boldsymbol{x}, \omega) \mapsto \boldsymbol{C}(\boldsymbol{x}, \omega). \tag{2}$$

For later use, we define also the expected value for the random variable Z in Eq.(1) as, see e.g. Lasota and Mackey (1994),

$$\mathbb{E}(Z) = \int_{\Omega} Z d\mathbb{P} = \int_{\Omega} Z(\omega) d\mathbb{P}(\omega). \tag{3}$$

2.2 Governing Equations for an Elastic Body

In this paper we consider a linear elastic material behavior characterized by two fluctuating material input parameters. Therefore, as mentioned above, the elasticity tensor $\boldsymbol{C}(\boldsymbol{x}, \omega)$ becomes a stochastic field. In summary, based on the known equations in continuum mechanics, the following governing equations are used:

$$\begin{aligned} &1.\quad \nabla \cdot \boldsymbol{\sigma}(\boldsymbol{x}, \omega) = \boldsymbol{0} \\ &2.\quad \boldsymbol{\sigma}(\boldsymbol{x}, \omega) = \boldsymbol{C}(\boldsymbol{x}, \omega) : \boldsymbol{\varepsilon}(\boldsymbol{x}, \omega) \\ &3.\quad \boldsymbol{\varepsilon}(\boldsymbol{x}, \omega) = \frac{1}{2}(\nabla \boldsymbol{u}(\boldsymbol{x}, \omega) + (\nabla \boldsymbol{u}(\boldsymbol{x}, \omega))^T). \end{aligned} \tag{4}$$

In addition to the elasticity tensor $\boldsymbol{C}$ we have: $\boldsymbol{\sigma}$ is the Cauchy stress tensor, $\boldsymbol{u}$ is the system response- (respectively displacement) vector, $\boldsymbol{\varepsilon}$ is the strain tensor and ∇ denotes the standard Nabla operator. For the position vector $\boldsymbol{x} \in R$ holds, where $R \subset \mathbb{R}^3$ is some bounded, admissible region of the elastic body with corresponding boundary ∂R. In Eq.(4.1) we neglect body forces. Dirichlet and Neumann boundary conditions are considered as

$$\boldsymbol{u} = \bar{\boldsymbol{u}} \text{ on } \partial R_u,\ \ \bar{\boldsymbol{t}} = \boldsymbol{\sigma} \cdot \boldsymbol{n} \text{ on } \partial R_\sigma \tag{5}$$

with non-intersecting boundaries $\partial R = \partial R_\sigma \cup \partial R_u$ and $0 = \partial R_\sigma \cap \partial R_u$.

We remark that each system property like boundary conditions, external forces, geometry etc. may have an uncertainty. However, in this work we focus on the parameter uncertainty for the elasticity tensor $\boldsymbol{C}$ according to Eq.(2) such that the displacement vector $\boldsymbol{u}(\boldsymbol{x},\omega)$, the stress tensor $\boldsymbol{\sigma}(\boldsymbol{x},\omega)$ and the strain tensor $\boldsymbol{\varepsilon}(\boldsymbol{x},\omega)$ become stochastic fields.

2.3 Variational Formulation

In addition to the spatial integration, a stochastic integration over the stochastic domain is introduced, thus resulting into the following weak form:

$$\int_\Omega \int_R \delta\boldsymbol{\varepsilon}(\boldsymbol{x},\omega) : \boldsymbol{C}(\boldsymbol{x},\omega) : \boldsymbol{\varepsilon}(\boldsymbol{x},\omega) dR d\mathbb{P} = \int_\Omega \int_{\partial R_\sigma} \bar{\boldsymbol{t}}(\boldsymbol{x}) \delta\boldsymbol{u}(\boldsymbol{x},\omega) d\partial R d\mathbb{P}. \tag{6}$$

The aim is to find $\boldsymbol{u} \in R$ such that for all testfunctions $\delta\boldsymbol{u}$ Eq.(6) is satisfied. In order to decompose the deterministic and the purely fluctuating part the random variables are divided as

$$\begin{aligned} &1. \quad \boldsymbol{u}(\boldsymbol{x},\omega) = \bar{\boldsymbol{u}}(\boldsymbol{x}) + \widetilde{\boldsymbol{u}}(\boldsymbol{x},\omega) \\ &2. \quad \boldsymbol{\varepsilon}(\boldsymbol{x},\omega) = \bar{\boldsymbol{\varepsilon}}(\boldsymbol{x}) + \widetilde{\boldsymbol{\varepsilon}}(\boldsymbol{x},\omega) \\ &3. \quad \boldsymbol{C}(\boldsymbol{x},\omega) = \bar{\boldsymbol{C}}(\boldsymbol{x}) + \widetilde{\boldsymbol{C}}(\boldsymbol{x},\omega). \end{aligned} \tag{7}$$

In these relations each first term represents the deterministic part (expected value) and the second term the fluctuating part. With an analogous decomposition for $\delta\boldsymbol{u}(\boldsymbol{x},\omega)$ and $\delta\boldsymbol{\varepsilon}(\boldsymbol{x},\omega)$ Eq.(6) results into

$$\begin{aligned} &\overset{\mathbf{1}}{\int_R} \delta\bar{\boldsymbol{\varepsilon}}(\boldsymbol{x})^T : \bar{\boldsymbol{C}}(\boldsymbol{x}) : \bar{\boldsymbol{\varepsilon}}(\boldsymbol{x}) dR \quad + \quad \overset{\mathbf{2}}{\int_\Omega \int_R} \delta\widetilde{\boldsymbol{\varepsilon}}(\boldsymbol{x},\omega)^T : \bar{\boldsymbol{C}}(\boldsymbol{x}) : \bar{\boldsymbol{\varepsilon}}(\boldsymbol{x}) dR d\mathbb{P} \ldots \\ &+ \quad \overset{\mathbf{3}}{\int_\Omega \int_R} \delta\bar{\boldsymbol{\varepsilon}}(\boldsymbol{x})^T : \widetilde{\boldsymbol{C}}(\boldsymbol{x},\omega) : \bar{\boldsymbol{\varepsilon}}(\boldsymbol{x}) dR d\mathbb{P} \quad + \quad \overset{\mathbf{4}}{\int_\Omega \int_R} \delta\widetilde{\boldsymbol{\varepsilon}}(\boldsymbol{x},\omega)^T : \widetilde{\boldsymbol{C}}(\boldsymbol{x},\omega) : \bar{\boldsymbol{\varepsilon}}(\boldsymbol{x}) dR d\mathbb{P} \ldots \\ &+ \quad \overset{\mathbf{5}}{\int_\Omega \int_R} \delta\bar{\boldsymbol{\varepsilon}}(\boldsymbol{x})^T : \bar{\boldsymbol{C}}(\boldsymbol{x}) : \widetilde{\boldsymbol{\varepsilon}}(\boldsymbol{x},\omega) dR d\mathbb{P} \quad + \quad \overset{\mathbf{6}}{\int_\Omega \int_R} \delta\widetilde{\boldsymbol{\varepsilon}}(\boldsymbol{x},\omega)^T : \bar{\boldsymbol{C}}(\boldsymbol{x}) : \widetilde{\boldsymbol{\varepsilon}}(\boldsymbol{x},\omega) dR d\mathbb{P} \ldots \\ &+ \quad \overset{\mathbf{7}}{\int_\Omega \int_R} \delta\bar{\boldsymbol{\varepsilon}}(\boldsymbol{x})^T : \widetilde{\boldsymbol{C}}(\boldsymbol{x},\omega) : \widetilde{\boldsymbol{\varepsilon}}(\boldsymbol{x},\omega) dR d\mathbb{P} \quad + \quad \overset{\mathbf{8}}{\int_\Omega \int_R} \delta\widetilde{\boldsymbol{\varepsilon}}(\boldsymbol{x},\omega)^T : \widetilde{\boldsymbol{C}}(\boldsymbol{x},\omega) : \widetilde{\boldsymbol{\varepsilon}}(\boldsymbol{x},\omega) dR d\mathbb{P} \ldots \\ &\qquad = \quad \int_R \boldsymbol{f} \delta\bar{\boldsymbol{u}}(\boldsymbol{x}) dR + \int_\Omega \int_R \boldsymbol{f}(\boldsymbol{x}) \delta\widetilde{\boldsymbol{u}}(\boldsymbol{x},\omega) dR d\mathbb{P}. \end{aligned} \tag{8}$$

Compared to the terms $\mathbf{1}-\mathbf{7}$ the term $\mathbf{8}$ in Eq.(8) merely consists of purely fluctuating parts, and therefore will be neglected in the sequel. For numerical solution of the weak form in Eq.(8) the SFEM is used where spatial and stochastic discretization are applied as described next.

3 Spatial Discretization

Upon using Voigt's matrix notation on the element domain, we have the displacement approximation

$$\underline{u}(\underline{x},\omega) = \sum_{i=1}^{n_k} N_i(\underline{x}) u_i(\omega) = \underline{N}(\underline{x}) \underline{u}(\omega) \tag{9}$$

and the strain approximation

$$\underline{\varepsilon}(\underline{x},\omega) = \underline{B}(\underline{x}) \underline{u}(\omega), \tag{10}$$

where $\underline{B}$ is the associated derivative matrix of shape functions N_i. By applying the Galerkin projection, see e.g. Hackbusch (1989); Matthies and Keese (2005), the spatial part is

$$\underbrace{\mathop{\mathsf{A}}_{e=1}^{n_e} \int_{{}^eR} \underline{B}(\underline{x})^T \underline{C}(\underline{x},\omega)\underline{B}(\underline{x})dR\, \underline{u}(\omega)}_{\underline{K}} = \underbrace{\mathop{\mathsf{A}}_{e=1}^{n_e} \int_{\partial^eR} \bar{\underline{t}}(\underline{x})\underline{N}(\underline{x})dR,}_{\underline{f}} \tag{11}$$

where A is the assembly operator and ${}^eR$ is the region of one finite element. We denote

$$\underline{K}(\underline{x},\omega)\underline{u}(\omega) = \bar{\underline{f}}(\underline{x}) \tag{12}$$

as the semi-discrete form. In this context n_k is the number of nodes per element and n_e is the number of elements. Using the relations (7), Eq.(11) becomes

$$\begin{aligned} \mathop{\mathsf{A}}_{e=1}^{n_e} \int_{{}^eR} \underline{B}(\underline{x})^T \bar{\underline{C}}(\underline{x})\underline{B}(\underline{x})dR\bar{\underline{u}} \quad &+ \quad \mathop{\mathsf{A}}_{e=1}^{n_e} \int_{{}^eR} \underline{B}(\underline{x})^T \bar{\underline{C}}(\underline{x})\underline{B}(\underline{x})dR\widetilde{\underline{u}}(\omega)\ldots \\ + \quad \mathop{\mathsf{A}}_{e=1}^{n_e} \int_{{}^eR} \underline{B}(\underline{x})^T \widetilde{\underline{C}}(\underline{x},\omega)\underline{B}(\underline{x})dR\bar{\underline{u}} \quad &+ \quad \mathop{\mathsf{A}}_{e=1}^{n_e} \int_{{}^eR} \underline{B}(\underline{x})^T \widetilde{\underline{C}}(\underline{x},\omega)\underline{B}(\underline{x})dR\widetilde{\underline{u}}(\omega)\ldots \\ &= \quad \mathop{\mathsf{A}}_{e=1}^{n_e} \int_{{}^eR} \underline{f}(\underline{x})\underline{N}(\underline{x})dR \end{aligned} \tag{13}$$

or in a short decomposed form

$$(\underline{K}_0(\underline{x}) + \widetilde{\underline{K}}(\underline{x},\omega))(\bar{\underline{u}} + \widetilde{\underline{u}}(\omega)) = \bar{\underline{f}}. \tag{14}$$

In particular, $\underline{K_0}$ represents the deterministic part and respectively $\widetilde{\underline{K}}$ the fluctuating part:

$$\begin{aligned} &1. \qquad \underline{K}_0(\underline{x}) = \mathop{\mathsf{A}}_{e=1}^{n_e} \int_{{}^eR} \underline{B}(\underline{x})^T \bar{\underline{C}}(\underline{x})\underline{B}(\underline{x})dR, \\ &2. \qquad \widetilde{\underline{K}}(\underline{x},\omega) = \mathop{\mathsf{A}}_{e=1}^{n_e} \int_{{}^eR} \underline{B}(\underline{x})^T \widetilde{\underline{C}}(\underline{x},\omega)\underline{B}(\underline{x})dR \end{aligned} \tag{15}$$

Eq.(13) is the starting point for the subsequent stochastic discretization.

4 Stochastic Discretization

In order to perform the stochastic discretization we first have to introduce the multi-variate Hermite polynomials and the polynomial chaos expansion. Similar to the spatial discretization the multi-variate Hermite polynomials serve as ansatzfunctions for the stochastic domain.

4.1 Multi-variate Hermite Polynomials

The multi-variate Hermite polynomials are defined by, Keese (2004); Luo (2006)

$$H_\alpha(\underline{\theta}) := \prod_{i\in\mathbb{N}} h_{\alpha_i}(\theta_i), \tag{16}$$

where $\alpha = (\alpha_1, \alpha_2, \ldots)$ is a multi-index and $\underline{\theta} = (\theta_1, \theta_2, \ldots)$ is the infinite vector of standard Gaussian random variables. In these relations h_{α_i} are the *probabilistic Hermite polynomials*. The first six terms have the following form:

$$\begin{aligned} h_0(\theta) &= 1 & h_3(\theta) &= \theta^3 - 3\theta \\ h_1(\theta) &= \theta & h_4(\theta) &= \theta^4 - 6\theta + 3 \\ h_2(\theta) &= \theta^2 - 1 & h_5(\theta) &= \theta^5 - 10\theta^3 + 15\theta. \end{aligned} \tag{17}$$

Due to orthogonality of the polynomials it follows, Luo (2006):

$$\mathbb{E}(H_0) = 1, \qquad \mathbb{E}(H_\alpha H_\beta) = \delta_{\alpha\beta}, \qquad \mathbb{E}(H_\alpha) = 0 \quad \forall \alpha \neq 0, \tag{18}$$

where $\mathbb{E}(H_\alpha)$ denotes the expected value of H_α according to Eq.(3).

4.2 Wiener's Polynomial Chaos

The exact Polynomial Chaos Representation (PCE) of the random variable $\underline{u}(\omega)$ in (12) is written as

$$\underline{u}(\omega) = \underline{u}(\underline{\theta}(\omega)) = \sum_{\alpha \in J} \underline{u}_\alpha H_\alpha(\underline{\theta}(\omega)), \tag{19}$$

respectively

$$\underline{C}(\underline{x}, \omega) = \underline{C}(\underline{x}, \underline{\theta}(\omega)) = \sum_{\alpha \in J} \underline{C}_\alpha(\underline{x}) H_\alpha(\underline{\theta}(\omega)) \tag{20}$$

for the locally dependent elasticity matrix with J as an infinite set of indices.

To discretize the random fields in the SPDE, a representation into a finite number of mutually independent standard normally distributed random variables $\underline{\hat{\theta}} = (\theta_1, \theta_2, \ldots, \theta_m)$ is applied, Matthies and Keese (2005). The approximated representation which is important for the numerical computation is then written as

$$\underline{u}(\omega) \approx \underline{u}(\underline{\hat{\theta}}) = \sum_{\alpha \in \hat{J}} \underline{u}_\alpha H_\alpha(\underline{\hat{\theta}}) \tag{21}$$

$$\underline{C}(\underline{x}, \omega) \approx \underline{C}(\underline{x}, \underline{\hat{\theta}}) = \sum_{\alpha \in \hat{J}} \underline{C}_\alpha(\underline{x}) H_\alpha(\underline{\hat{\theta}}) \tag{22}$$

with $\hat{J}$ as a finite set of indices, Matthies and Keese (2005). In this context, we should note that $\underline{u}_0 = \bar{\underline{u}}$ and $\underline{C}_0(\underline{x}) = \bar{\underline{C}}(\underline{x})$ applies, i.e. we obtain the expected values.

4.3 PCE of a Two Parameter Model

As a special case of linear elasticity we consider a linear elastic isotropic material described by two stochastic independent material parameters. Furthermore, the considered material is regarded as homogeneous with respect to the expected value, that is, the variances of the input parameters are assumed to be identical for each location. Therefore, for the subsequent analysis we can neglect the spatial dependence in $\underline{C}(\underline{x})$. Furthermore we assume that the input parameters are Gaussian which is also verified by the experimental data used in the example in Section 5.

The elasticity matrix for a linear isotropic material is given as

$$\underline{C} = \underline{C}_{dev} + \underline{C}_{vol} = 2G\underline{I}^C_{dev} + K\underline{m}\underline{m}^T \tag{23}$$

with

$$\begin{aligned} &1. \quad G = \frac{E}{2(1+\nu)} \quad \text{shear modulus,} \\ &2. \quad K = \frac{E}{3(1-2\nu)} \quad \text{bulk modulus} \end{aligned} \tag{24}$$

and

$$\underline{I}^C_{dev} = \underline{I}^C - \frac{1}{3}\underline{m}\underline{m}^T, \qquad \underline{I}^C = \begin{bmatrix} 1 & & & & & & \\ & 1 & & & & & \\ & & 1 & & & & \\ & & & \frac{1}{2} & & & \\ & & & & \frac{1}{2} & & \\ & & & & & \frac{1}{2} & \\ & & & & & & \frac{1}{2} \end{bmatrix}, \qquad \underline{m} = \begin{bmatrix} 1 \\ 1 \\ 1 \\ 0 \\ 0 \\ 0 \end{bmatrix}. \tag{25}$$

By use of the Gaussian random variables $G(\omega) = G_0 + G_1\theta_1(\omega)$ and $K(\omega) = K_0 + K_1\theta_2(\omega)$ we obtain the stochastic elasticity matrix

$$\begin{aligned} \underline{C}(\underline{\hat{\theta}}) &= 2(G_0 + G_1\theta_1)\underline{I}^C_{dev} + (K_0 + K_1\theta_2)\underline{m}\underline{m}^T \\ &= \underbrace{2G_0\underline{I}^C_{dev} + K_0\underline{m}\underline{m}^T}_{\underline{C}_0} + \underbrace{2G_1\underline{I}^C_{dev}}_{\underline{C}_1}\theta_1 + \underbrace{K_1\underline{m}\underline{m}^T}_{\underline{C}_2}\theta_2 \\ &= \underline{C}_0 + \underline{C}_1\theta_1 + \underline{C}_2\theta_2. \end{aligned} \tag{26}$$

Eq.(26) constitutes a PCE of the elasticity matrix. Since we assume the random variables G and K as normally distributed the PCE consists of two summands, each associated with one standard Gaussian random variable θ_i. For this reason we may represent their PCE with *normal* indices instead of multi-indices. Consequently, the system response depends also on two standard Gaussion random variables:

$$\underline{\mathbf{u}}(\hat{\underline{\theta}}) = \underline{u}_0 + \underline{u}_1\theta_1 + \underline{u}_2\theta_2 \tag{27}$$

4.4 Galerkin Projection

Now we use the expansions (26) and (27) and apply the Galerkin projection explained in Hackbusch (1989); Matthies and Keese (2005) on Eq.(13):

$$\begin{aligned}
&\mathsf{A}_{e=1}^{n_e} \int_\Omega H_\beta(\hat{\underline{\theta}}) \int_{{}^eR} \underline{B}(\underline{x})^T \underline{C}_0 \underline{B}(\underline{x}) dR d\mathbb{P} \underline{u}_0 \dots \\
&+ \mathsf{A}_{e=1}^{n_e} \int_\Omega H_\beta(\hat{\underline{\theta}}) \int_{{}^eR} \underline{B}(\underline{x})^T \underline{C}_0 \underline{B}(\underline{x}) dR \left(\underline{u}_1\theta_1 + \underline{u}_2\theta_2\right) d\mathbb{P} \dots \\
&+ \mathsf{A}_{e=1}^{n_e} \int_\Omega H_\beta(\hat{\underline{\theta}}) \int_{{}^eR} \underline{B}(\underline{x})^T \left(\underline{C}_1\theta_1 + \underline{C}_2\theta_2\right) \underline{B}(\underline{x}) dR d\mathbb{P} \underline{\bar{u}} \dots \\
&+ \mathsf{A}_{e=1}^{n_e} \int_\Omega H_\beta(\hat{\underline{\theta}}) \int_{{}^eR} \underline{B}(\underline{x})^T \left(\underline{C}_1\theta_1 + \underline{C}_2\theta_2\right) \underline{B}(\underline{x}) dR \left(\underline{u}_1\theta_1 + \underline{u}_2\theta_2\right) d\mathbb{P} \\
&\qquad = \mathsf{A}_{e=1}^{n_e} \int_\Omega H_\beta(\hat{\underline{\theta}}) \int_{{}^eR} \underline{f}(\underline{x}) \underline{N}(\underline{x}) dR d\mathbb{P} \;\; \forall \beta \in \hat{J}.
\end{aligned} \tag{28}$$

By exploiting the Hermite polynomial properties of Eq.(18) with Eq.(3) and neglecting term $\mathbf{8}$ in Eq.(8) it follows for Eq.(28):

$$\begin{aligned}
\beta = 0 \quad &\rightarrow \quad \underline{K}_0\underline{u}_0 + \underline{K}_1\underline{u}_1 + \underline{K}_2\underline{u}_2 + \dots && = \underline{f}_0 \neq \underline{0} \\
\beta = 1 \quad &\rightarrow \quad \underline{K}_0\underline{u}_1 + \underline{K}_1\underline{u}_0 && = \underline{f}_1 = \underline{0} \\
\beta = 2 \quad &\rightarrow \quad \underline{K}_0\underline{u}_2 + \underline{K}_2\underline{u}_0 && = \underline{f}_2 = \underline{0}
\end{aligned}$$

with

$$\begin{aligned}
&1.\;\; \underline{K}_0 = \mathsf{A}_{e=1}^{n_e} \int_{{}^eR} \underline{B}(\underline{x})^T \underline{C}_0 \underline{B}(\underline{x}) dR \\
&2.\;\; \underline{K}_1 = \mathsf{A}_{e=1}^{n_e} \int_{{}^eR} \underline{B}(\underline{x})^T \underline{C}_1 \underline{B}(\underline{x}) dR \\
&3.\;\; \underline{K}_2 = \mathsf{A}_{e=1}^{n_e} \int_{{}^eR} \underline{B}(\underline{x})^T \underline{C}_2 \underline{B}(\underline{x}) dR
\end{aligned} \tag{29}$$

In matrix notation we obtain

$$1.\;\; \underline{\mathbf{K}}\underline{\mathbf{u}} = \underline{\mathbf{f}}, \;\; \text{where} \;\; 2.\;\; \underbrace{\begin{bmatrix} \underline{K}_0 & \underline{K}_1 & \underline{K}_2 \\ \underline{K}_1 & \underline{K}_0 & \underline{0} \\ \underline{K}_2 & \underline{0} & \underline{K}_0 \end{bmatrix}}_{\underline{\mathbf{K}}} \underbrace{\begin{bmatrix} \underline{u}_0 \\ \underline{u}_1 \\ \underline{u}_2 \end{bmatrix}}_{\underline{\mathbf{u}}} = \underbrace{\begin{bmatrix} \underline{f}_0 \\ \underline{0} \\ \underline{0} \end{bmatrix}}_{\underline{\mathbf{f}}}. \tag{30}$$

Eq.(30) constitutes a deterministic system of equations. Each $\underline{K}_\alpha$ in Eq.(29) and Eq.(30), respectively, are obtained as in the standard finite element method. The solution vector $\underline{u}$ in Eq.(30) represents the PC-coefficients for the displacement. It is used to determine the density function of $\underline{\mathbf{u}}(\underline{\boldsymbol{\theta}})$ and thereby compute the statistics.

4.5 Numerical Implementation

A common feature of the standard FEM is the banded structure of the stiffness matrix, which also holds for the stiffness matrices $\underline{K}_0$, $\underline{K}_1$ and $\underline{K}_2$ in Eq.(30). However, in general this does not imply a banded structure for the total matrix $\underline{\mathbf{K}}$ in Eq.(30). Therefore, for large sized problems a direct solver is not practical for solution of $\underline{\boldsymbol{u}}$ and consequently we use an iterative scheme with a *preconditioned gradient method* as follows, Saad (2003):

$$\underline{\mathbf{u}}_{n+1} = \underline{\mathbf{u}}_n - \tilde{\underline{\mathbf{K}}}^{-1}\underline{\mathbf{R}}(\underline{\mathbf{u}}_n) \tag{31}$$

with

$$1.\ \underline{\mathbf{R}}(\underline{\mathbf{u}}_n) = \underline{\mathbf{K}}\underline{\mathbf{u}}_n - \underline{\mathbf{f}}, \quad 2.\ \tilde{\underline{\mathbf{K}}} = \begin{bmatrix} \underline{K}_0 & \underline{0} & \underline{0} \\ \underline{0} & \underline{K}_0 & \underline{0} \\ \underline{0} & \underline{0} & \underline{K}_0 \end{bmatrix}. \tag{32}$$

Figure 1 illustrates the iterative scheme for the linear elastic SFEM, compared to the standard linear elastic FEM. It becomes obvious, that for the SFEM with two independent normally distributed parameters, two additionally loops become necessary. In this way, an increase of independent parameters and/or the order of their PCE (for non-Gaussian input parameters for example) results to an increase of the number m for the matrices $\underline{C}_i$ and respectively $\underline{K}_i$, $i = 1, ..., m$.

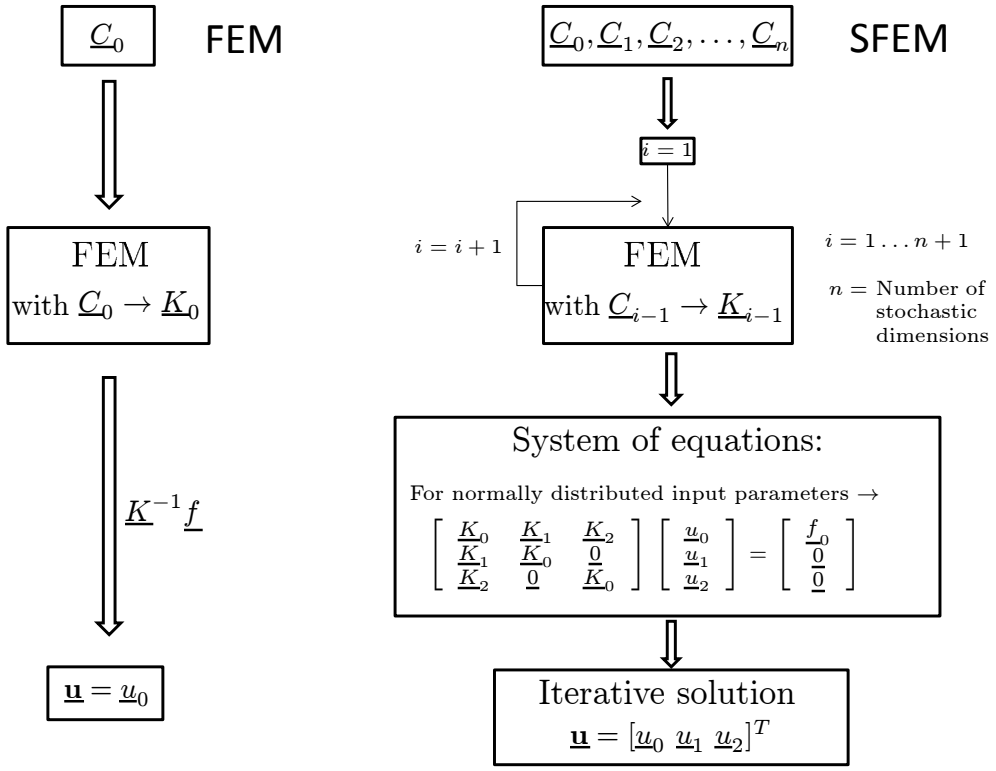

Figure 1: Comparison between FEM and SFEM

5 Representative Example

This section illustrates some stochastic properties of our two parameter model of the previous section for a plate with a ring hole in a numerical example. The geometry, its loading and the FE-discretization are depicted in Figure 2. The loading is $\bar{t} = 200$ N/m. For symmetry reasons only a quarter of the structure is investigated, as marked in Figure 2.b. Note, that in this way we tacitly assume also a symmetry for the stochastic discretization.

We consider two different cases. Case I is based on the assumption that *Youngs modulus* and *Poisson's ratio* are two given independent parameters, which means, that the distributions (respectively the density functions) of $E(\omega)$ and $\nu(\omega)$ are assumed to be known. Case II assumes a known distribution for the shear modulus $G(\omega)$ instead for

Poisson's ratio $\nu(\omega)$. In both cases, the additional dependent elasticity parameters are calculated in terms of the independent parameters. The material under consideration, which provides the experimental data, is an adhesive material. Experimental observations of this material are published in Nörenberg and Mahnken (2013) for combined tension torsion tests.

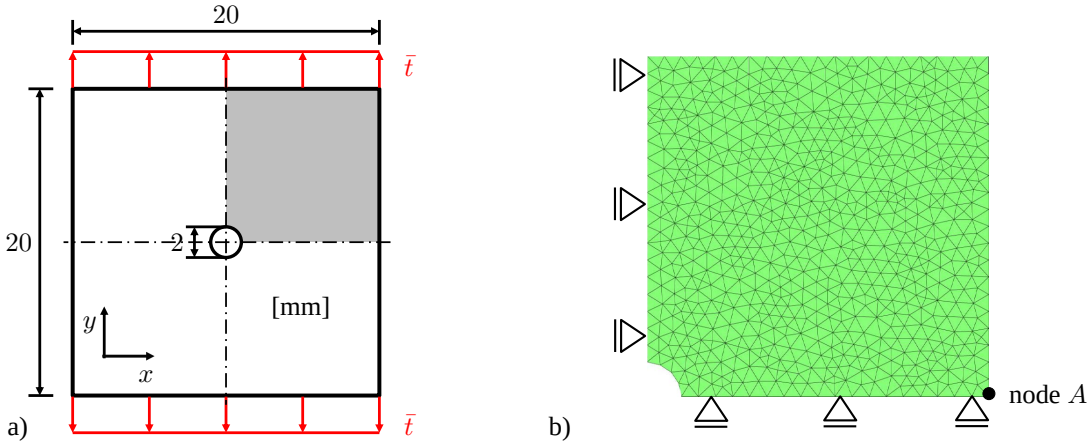

Figure 2: Plate with a ring hole: a) Geometry and b) finite element mesh of triangular elements

5.1 Case I: E and ν are Stochastically Independent Parameters

We assume Young's modulus $E(\omega)$ and Poisson's ratio $\nu(\omega)$ as stochastically independent parameters with known density functions. One general framework for statistical analysis in this work is the generation of synthetic data. Thus, to ensure more reliable results we use synthetic data for combined tension torsion tests, generated based on experimental data as published in Nörenberg and Mahnken (2013). For this, a non-linear regression model in combination with an autoregressive moving average process (ARMA) is used. The regression model is an approximation of the experimental data dependent on a non-linear regression function with a finite number of fitting parameters, whereas the ARMA model describes the residuals between the experimental data and the fitted regression function. The resulting density functions for E and ν in Figure 3 demonstrate both random variables almost as normally distributed. Therefore we can apply the relations

$$\begin{aligned} &1. \quad E(\theta_1) = E_0 + E_1\theta_1 \\ &2. \quad \nu(\theta_2) \ = \nu_0 + \nu_1\theta_2, \end{aligned} \tag{33}$$

where θ_1 and θ_2 are the corresponding Gaussian random variables and the corresponding values for the coefficients are:

$$\begin{aligned} &1. \quad E_0 = 1427 \text{ MPa}, \quad E_1 = 145 \text{ MPa} \\ &2. \quad \nu_0 \ = 0.337, \qquad\quad \nu_1 = 0.062. \end{aligned} \tag{34}$$

Here, E_0 and ν_0 represent the expected values and E_1 and ν_1 the corresponding deviations for both random variables.

We point out again, that the random variables in Eq.(33) can be represented by PCEs with two summands, which is due to the normal distributions of both parameters in Figure 3.

Next, we calculate the density functions of two additional parameters $G(\omega)$ and $K(\omega)$ in Eq.(24). To this end we use a common result from statistics that for two independent random variables X_1 and X_2 with associated density functions f_{X_1} and f_{X_2} the distribution density of the quotient f_{X_1/X_2} is then given by, see e.g. Dominique and Aime (1999)

$$f_{X_1/X_2}(z) = \int_{\mathbb{R}} |t| f_{X_1}(zt) f_{X_2}(t) dt. \tag{35}$$

Applying Eq.(35) to Eq.(24) we obtain the shear and the bulk modulus, which are stochastically dependent on E and ν:

$$G(\omega) \approx \frac{E(\theta_1)}{2(1+\nu(\theta_2))}, \qquad K(\omega) \approx \frac{E(\theta_1)}{3(1-2\nu(\theta_2))}. \tag{36}$$

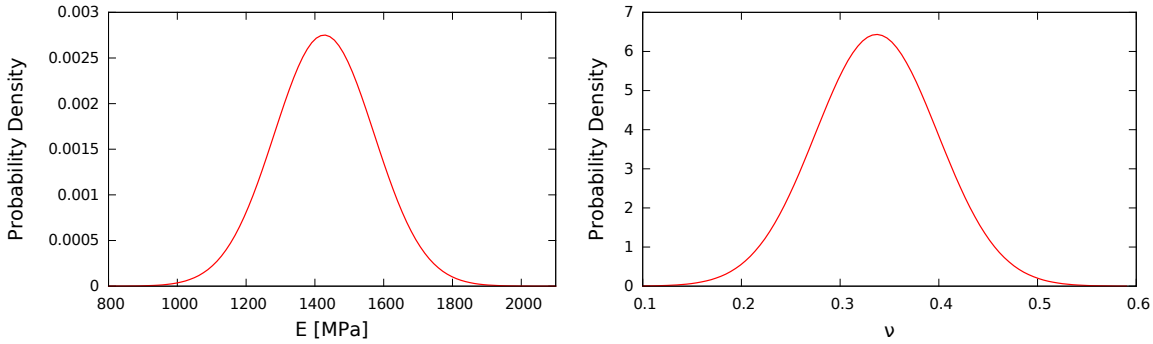

(a) Density function for *Young's modulus*

(b) Density function for *Poisson's ratio*

Figure 3: Case I: Density functions for stochastically independent parameters generated from synthetic data

Figure 4 shows the corresponding density functions. Whereas G has a Gaussian distribution, the distribution for K is non-Gaussian. However, in the sequel for simplicity we will use a Gaussian representation for K, thus resulting into

$$\begin{aligned} &1. \quad G(\theta_1') = G_0 + G_1\theta_1' \\ &2. \quad K(\theta_2') = K_0 + K_1\theta_2' \end{aligned} \tag{37}$$

where θ_1' and θ_2' are the corresponding Gaussian random variables. The corresponding values are

$$\begin{aligned} &1. \quad G_0 = 534 \text{ MPa}, \quad G_1 = 60 \text{ MPa} \\ &2. \quad K_0 = 1459 \text{ MPa}, \quad K_1 = 450 \text{ MPa}. \end{aligned} \tag{38}$$

Using the Gaussian random variables G and K and the corresponding decomposition (26), we obtain the solution according to the iterative scheme in Eq.(31). Figure 5 shows the contour plot for the PC-coefficients of the displacement vector $\underline{\mathbf{u}} = [\underline{u}_0\ \underline{u}_1\ \underline{u}_2]^T$. In this context $\underline{u}_0$ represents the expected value, $\underline{u}_1$ the deviatoric fluctuation and $\underline{u}_2$ the volumetric fluctuation in x- and y-direction. As one can see, the fluctuating parts have a much smaller value (by a factor of 10) then the deterministic parts (expected value).

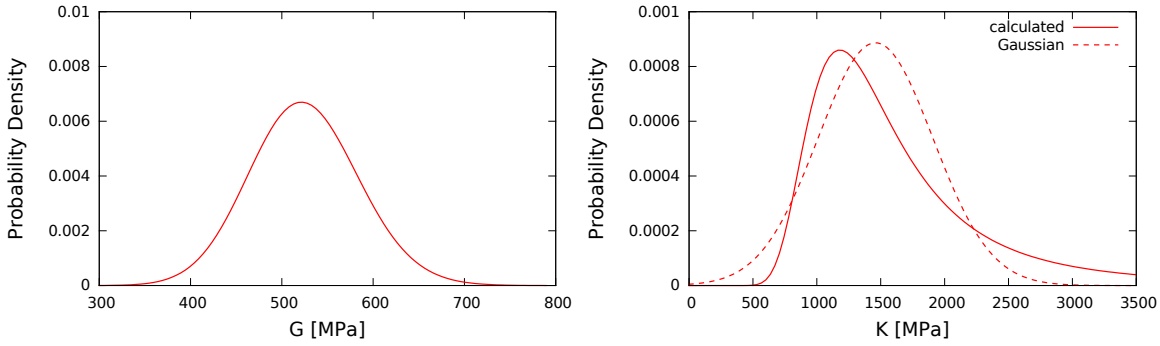

(a) Density function for the *shear modulus*

(b) Density function for the *bulk modulus*

Figure 4: Case I: Density functions for stochastically dependent parameters generated from Eq.(35) and Eq.(36), Figure (b) also shows the simplified Gaussian density function for K with the same variance as for the non-Gaussian density.

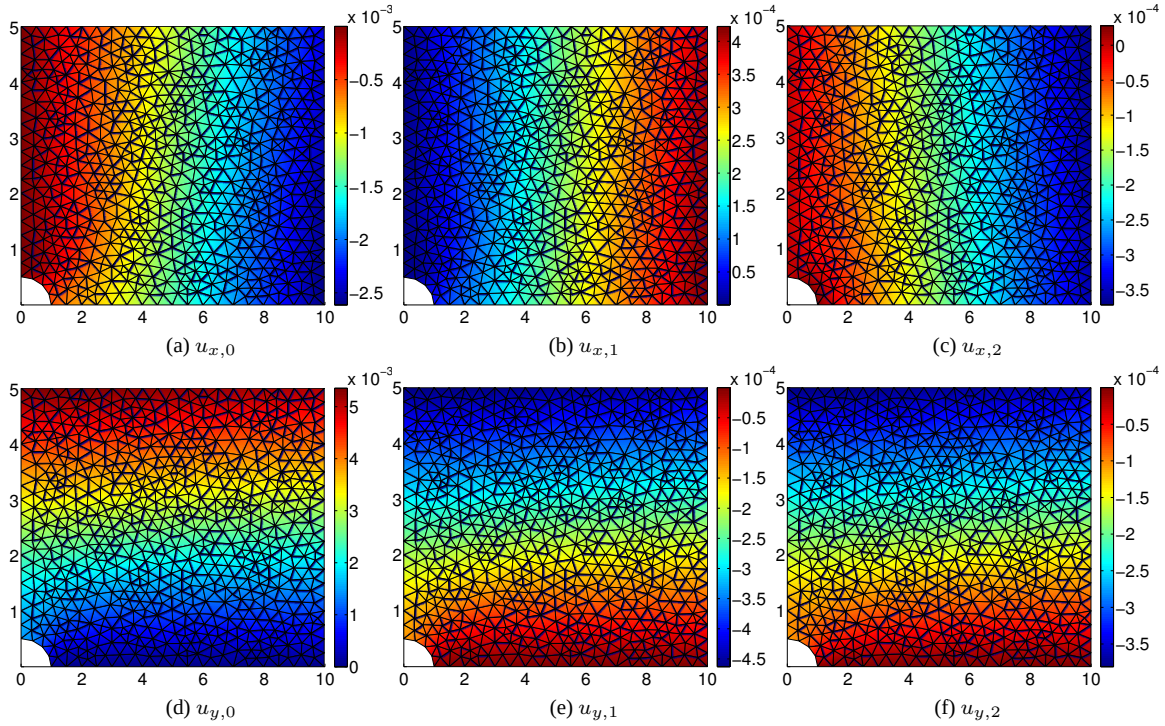

(a) $u_{x,0}$ (b) $u_{x,1}$ (c) $u_{x,2}$

(d) $u_{y,0}$ (e) $u_{y,1}$ (f) $u_{y,2}$

Figure 5: Case I: PC-coefficients for displacements in x- and y-direction.

5.2 Case II: E and G are Stochastically Independent Parameters

In the second case we assume Young's modulus $E(\omega)$ and the shear modulus $G(\omega)$ as stochastically independent input material parameters with known density functions. For this reason, Eq.(24.1) can be expressed as $\nu = \frac{E}{2G} - 1$. That means, ν becomes dependent on E and G, since in the linear isotropic case we always have only two independent material parameters. The resulting density functions for E and G in Figure 6 demonstrate both random variables almost as normally distributed. Therefore, analogously to Eq. (33) we can apply the relations

$$\begin{aligned} &1. \quad E(\theta_1) = E_0 + E_1\theta_1 \\ &2. \quad G(\theta_2) = G_0 + G_1\theta_2 \end{aligned} \tag{39}$$

with the corresponding values

$$\begin{aligned} &1. \quad E_0 = 1427 \text{ MPa}, \quad E_1 = 145 \text{ MPa} \\ &2. \quad G_0 = 545 \text{ MPa}, \quad G_1 = 43 \text{ MPa}. \end{aligned} \tag{40}$$

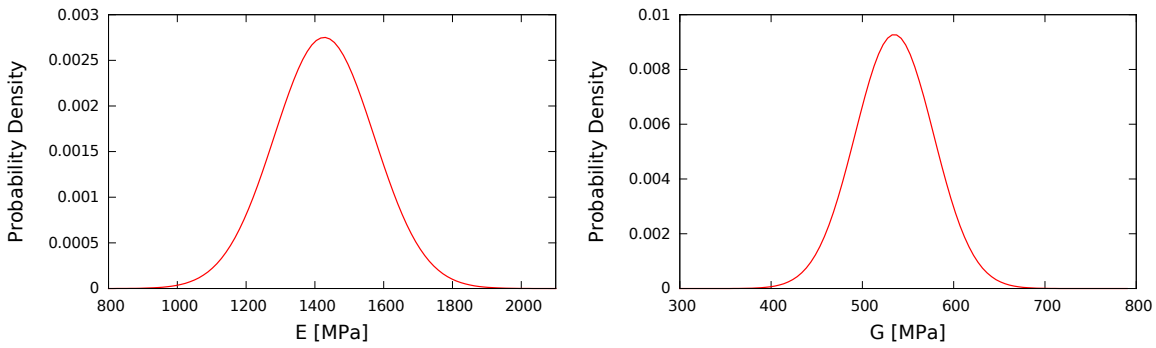

(a) Density function for *Young's modulus* (b) Density function for *shear modulus*

Figure 6: Case II: Density functions for stochastically independent parameters generated from synthetic data.

Rearranging the equations (24) results into

$$1.\ \nu(\omega) \approx \frac{E(\theta_1)}{2G(\theta_2)} - 1, \quad 2.\ K(\omega) \approx \frac{G(\theta_2)E(\theta_1)}{3(3G(\theta_2) - E(\theta_1)))} \approx \frac{E(\theta_1)}{3(1 - 2\nu(\underline{\hat{\theta}}))}. \tag{41}$$

Eq.(41.2) offers two approaches for determination of K. To avoid the multiplication of the random variables in the numerator and the division of the random variables in the denominator, we choose the second approach, that is, we use the expression of ν with the independent variables E and G in order to enable the calculation of K by aid of Eq. (36). In addition, a comparison of the experimental density function of ν in Case I and the (calculated) density function in Case II is possible.

Figure 7 shows the corresponding density functions. In this case, the *bulk modulus* is almost Gaussian. The smaller variance of K in Figure 7 (compared to Figure 4) can be explained by the fact that the variation of the calculated *Poisson's ratio* in Figure 7 (which is used for the determination of K) is smaller than for Case I. This is a consequence of the computation of ν with a less distributed *shear modulus* G. Also, the measured values of G in Case II may be determined more precisely than those of ν in Case I, which is the reason for the higher variation of ν and subsequently for K in Case I.

Since both quantities have a Gaussian distribution we use the representation

$$\begin{aligned} 1. \quad & \nu(\theta_1') = \nu_0 + \nu_1\theta_1' \\ 2. \quad & K(\theta_2') = K_0 + K_1\theta_2' \end{aligned} \tag{42}$$

with the corresponding values

$$\begin{aligned} 1. \quad & \nu_0 = 0.33, && \nu_1 = 0.029 \\ 2. \quad & K_0 = 1252 \text{ MPa}, && K_1 = 220 \text{ MPa}. \end{aligned} \tag{43}$$

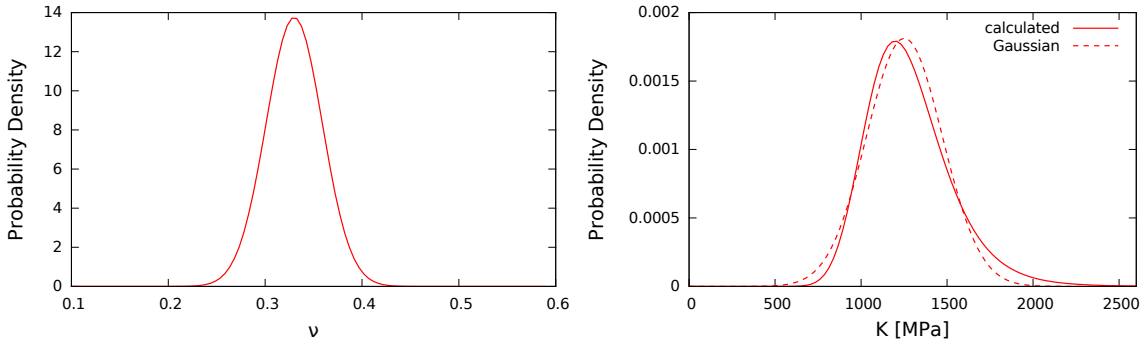

(a) Density function of *Poisson's ratio*

(b) Density function of *bulk modulus*

Figure 7: Case II: Density functions for stochastically dependent parameters generated from Eq.(35) and Eq.(41); (b) also shows the simplified Gaussian density function for K with the same variance as for the non-Gaussian density.

Figure 8 shows the contour plot for the PC-coefficients of the displacement vector $\underline{\mathbf{u}} = [\underline{u}_0\ \underline{u}_1\ \underline{u}_2]^T$.

5.3 Comparison of Case I and Case II

Table 1 presents the number of iterations for the preconditioned gradient method summarized in the equations (31). The tolerance for the accuracy of $||\underline{\mathbf{R}}(\underline{\mathbf{u}})||$ was chosen as $tol = 5 \cdot 10^{-9}$ for both cases. As can be seen, 15 iterations become necessary for Case I in order to achieve the same tolerance as for Case II with 11 iterations. The reason for this is the large deviation of the independent parameter $\nu(\omega)$ and the resulting deviation on the dependent parameters. Case II considers G instead of ν as an input parameter. The experimental values of G are much more accurate and the deviation is minor. As a consequence, less iterations become necessary.

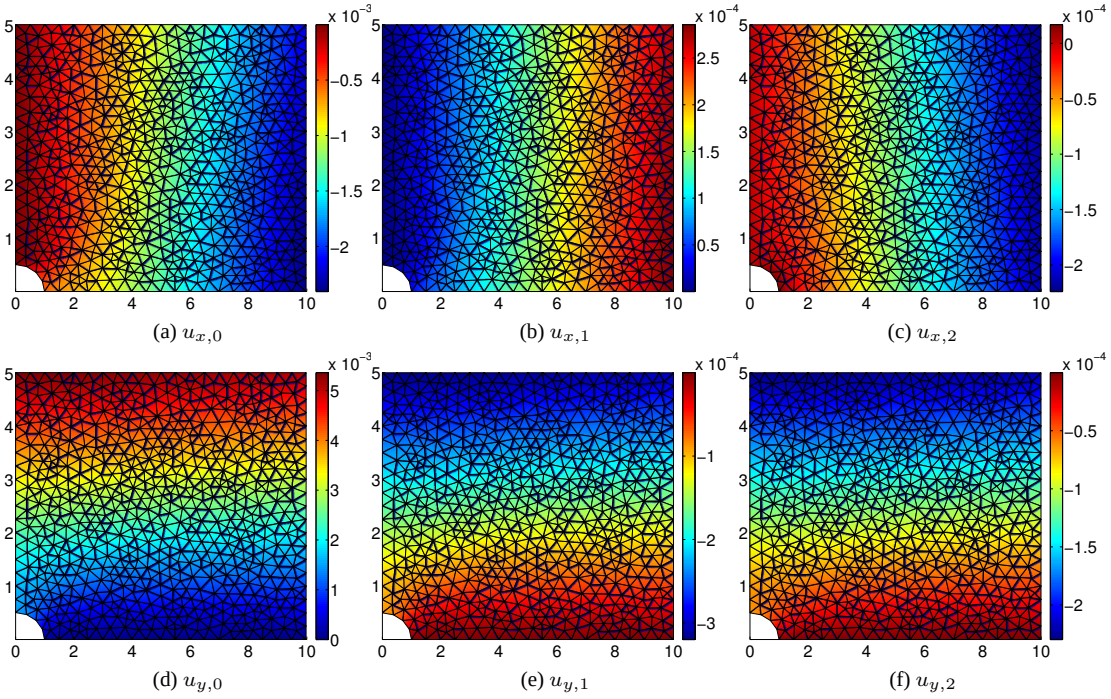

(a) $u_{x,0}$ (b) $u_{x,1}$ (c) $u_{x,2}$

(d) $u_{y,0}$ (e) $u_{y,1}$ (f) $u_{y,2}$

Figure 8: Case II: PC-coefficients for displacements in x- and y-direction.

Iterations	Case I	Case II
1	$2.119622607e-01$	$2.1196226079e-01$
2	$4.780679675e-02$	$2.773368156e-02$
⋮	⋮	⋮
10	$1.447632680e-06$	$7.686034244e-09$
11	$3.978522991e-07$	$1.180290246e-09$
12	$1.093495508e-07$	
13	$3.005583969e-08$	
14	$8.261535020e-09$	
15	$2.270964000e-09$	

Table 1: Residuals of the preconditioned gradient method for Case I and Case II with $tol = 5 \cdot 10^{-9}$

In the following we compare the displacement density functions of node A (shown in Figure 2.b) for both cases in x-direction. After the computation of $\underline{\mathbf{u}} = [\underline{u}_0\ \underline{u}_1\ \underline{u}_2]^T$ we are able to express it in the form (27). By numerical calculation or by analytical *convolution* we obtain the density functions for node A in x-direction shown in Figure 9. As becomes apparent, with large variance in the input parameters the calculated solution also obtains a large variance. That is, *„bad"* (or insufficient) measured values for the input parameters (in this case for $\nu(\omega)$) lead to a more scattered solution.

In summary the comparison of both cases illustrates the advantage of independent parameters with an accurate distribution with smaller variance over less accurate distributions with higher variance with respect to the iterative solution behavior and reliability.

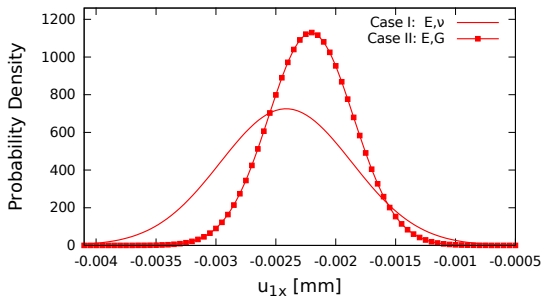

Figure 9: Comparison of density functions for Case I and Case II for node A in x-direction

6 Conclusion and Outlook

We have presented a general approach for solving stochastic partial differential equations (SPDEs) in the linear elastic case with the stochastic finite element method (SFEM). To this end the SPDE is discretized in the spatial domain (with the standard finite element method) and in the stochastic domain. For discretization in the stochastic domain we use the Polynomial Chaos Expansion (PCE) which divides the random fields in deterministic and stochastic parts. The final equation system is build for two stochastic independent Gaussian input parameters. This equation system consists of three stiffness matrices $\underline{K}_0$, $\underline{K}_1$ and $\underline{K}_2$ resulting from the decomposition of the elasticity matrix $\underline{C}$ in a deviatoric and a volumetric part. Here, $\underline{K}_0$ describes the deterministic part (expected value), $\underline{K}_1$ the deviatoric fluctuation and $\underline{K}_2$ the volumetric fluctuation. We compare two different cases for input parameters. In Case I we assume the distribution of *Young's modulus* E and *Poisson's ratio* ν to be known and independent. Case II considers the distribution of the *shear modu- lus* G to be known instead of ν. In both cases, further dependent parameters are calculated in terms of the independent parameters.

In the representative example, the experimental values for ν in Case II are less accurate compared to G in Case I, which ensues a larger variance for the density function of ν as for G. As a result, the density function of the displacement vector $\underline{\mathbf{u}}$ has a larger variance for Case II as for Case I. The contour plots of the PC-coefficients for the displacements resulting from the numerical simulation of a *plate with a ring hole* illustrate the expected values and the fluctuation of $\underline{\mathbf{u}}$ as a consequence of the fluctuation for the respective independent parameters. In summary we conclude, that a larger variance in the indepenent parameters results into a larger variance of the FE-results.

Since we have independent experimental measurements, the input parameters are considered as stochastically independent. However, in general they might correlate with each other. This possibility will be considered in future work where we will expand the procedure of this paper to the nonlinear case. Correlation coefficients of paired input parameters (which are given by experimental data) will be determined in order to get an accurate solution. Our further attempt is to focus on hybrid materials where we will have different material spatial domains. The goal is, eventually to compute statistics of the solution, e.g. compute probabilities, to exceed some threshold at an interface.

Acknowledgements The financial support of this research by the German NRW Fortschrittskolleg "Leicht-Effizient-Mobil", Institut für Leichtbau mit Hybridsystemen (ILH), is gratefully acknowledged.

References

Dominique, F.; Aime, F.: *Wahrscheinlichkeitsrechnung*. Birkhäuser, Basel (1999).

Feng, J.; Cen, S.; Li, C.; Owen, D.: Statistical reconstruction and Karhunen–Loève expansion for multiphase random media. *International Journal for Numerical Methods in Engineering*, 105, 1, (2016), 3–32.

Ghanem, R. G.; Spanos, P. D.: *Stochastic Finite Elements: A Spectral Approach*. Springer-Verlag, New York (1991).

Ghanem, R. G.; Spanos, P. D.: A stochastic Galerkin expansion for nonlinear random vibration analysis. *Probabilistic Engineering Mechanics*, 8, 3, (1993), 255–264.

Graham, L.; Deodatis, G.: Response and eigenvalue analysis of stochastic finite element systems with multiple correlated material and geometric properties. *Probabilistic Engineering Mechanics*, 16, 1, (2001), 11–29.

Hackbusch, W.: *Integralgleichungen: Theorie und Numerik*. Teubner, Stuttgard (1989).

Hurtado, J.; Barbat, A.: Monte carlo techniques in computational stochastic mechanics. *Archives of Computational Methods in Engineering*, 5, 1, (1998), 3–29.

Keese, A.: *Numerical Solutions of Systems with Stochastic Uncertainties: A General Purpose Framework for Stochastic Finite Elements*. Mechanik-Zentrum, Technical University of Braunschweig (2004).

Lasota, A.; Mackey, M. C.: *Chaos, Fractals, and Noise. Stochastic aspects of Dynamics*. Springer-Verlag, New York (1994).

Liu, W. K.; Belytschko, T.; Mani, A.: Probabilistic finite elements for nonlinear structural dynamics. *Computer Methods in Applied Mechanics and Engineering*, 56, 1, (1986a), 61–81.

Liu, W. K.; Belytschko, T.; Mani, A.: Random field finite elements. *International Journal for Numerical Methods in Engineering*, 23, 10, (1986b), 1831–1845.

Luo, W.: *Wiener chaos expansion and numerical solutions of stochastic partial differential equations*. Ph.D. thesis, California Institute of Technology (2006).

Matthies, H. G.; Keese, A.: Galerkin methods for linear and nonlinear elliptic stochastic partial differential equations. *Computer Methods in Applied Mechanics and Engineering*, 194, 12, (2005), 1295–1331.

Nörenberg, N.; Mahnken, R.: A stochastic model for parameter identification of adhesive materials. *Archive of Applied Mechanics*, 83, (2013), 367–378.

Papadrakakis, M.; Papadopoulos, V.: Robust and efficient methods for stochastic finite element analysis using monte carlo simulation. *Computer Methods in Applied Mechanics and Engineering*, 134, 3, (1996), 325–340.

Saad, Y.: *Iterative methods for sparse linear systems*. Siam (2003).

Stefanou, G.: The stochastic finite element method: Past, present and future. *Computer Methods in Applied Mechanics and Engineering*, 198, 912, (2009), 1031 – 1051.

Sudret, B.; Der Kiureghian, A.: *Stochastic finite element methods and reliability: a state-of-the-art report*. Department of Civil and Environmental Engineering, University of California, Berkeley (2000).

Vanmarcke, E.: *Random Fields: Analysis and Synthesis*. MIT Press, Cambridge Massachusetts (1983).

Wang, X.-Y.; Cen, S.; Li, C.; Owen, D.: A priori error estimation for the stochastic perturbation method. *Computer Methods in Applied Mechanics and Engineering*, 286, (2015), 1–21.

Address: Alex Dridger, Dr. Ismail Caylak, Prof. Dr. Rolf Mahnken, Universität Paderborn, Warburger Str. 100, 33098 Paderborn, Germany
email: `Dridger@ltm.upb.de, Caylak@ltm.upb.de, Rolf.Mahnken@ltm.upb.de`